Applied Surface Science 491 (2019) 505–516

Contents lists available at ScienceDirect

Applied Surface Science

journal homepage: www.elsevier.com/locate/apsusc

Full length article

Sub-kilogram-scale synthesis of highly dispersible zirconia nanoparticles for hybrid optical resins

Xianglei He[a,b,1], Zhi Wang[a,1], Dan Wang[a,b,*], Feng Yang[c], Ruijie Tang[a,b], Jie-Xin Wang[a,b], Yuan Pu[a,b,*], Jian-Feng Chen[a,b]

[a] State Key Laboratory of Organic Inorganic Composites, Beijing University of Chemical Technology, Beijing 100029, China
[b] Research Center of the Ministry of Education for High Gravity Engineering and Technology, Beijing University of Chemical Technology, Beijing 100029, China
[c] Key Laboratory of Advanced Technology of Materials (Ministry of Education of China), School of Materials Science and Engineering, Southwest Jiaotong University, Chengdu, Sichuan 610031, China

ARTICLE INFO

Keywords:
Zirconia nanoparticles
Polyvinyl alcohol
Hybrid film
High refractive index
Colloids

ABSTRACT

We report the synthesis of highly dispersible zirconia (ZrO_2) nanoparticles in sub-kilogram-scale by hydrothermal process coupled with alkaline hydrogen peroxide (AHP) treatment, with detailed studies on the effects of experimental parameters. Under optimized experimental condition, which was hydrothermal reaction at 110 °C for 6 h with mole ratio of sodium hydrate to zirconium carbonate basic in reactants as 2.3, pure-phase cubic-ZrO_2 nanoparticles are obtained. Followed by AHP treatment of the ZrO_2 nanoparticles at 50 °C for 5 h in 0.4 M hydrogen peroxide and 4 M sodium hydrate, the dispersibility of ZrO_2 nanoparticles in aqueous suspension was enhanced due to the introduced Zr-OH groups on the surface. ZrO_2 nanodispersion with solid content of 37 wt% in aqueous solution exhibited a uniform hydrodynamic size of 14.15 ± 5.834 nm and was stable for over six months without significant aggregates. Transparent hybrid optical resins with tunable refractive index in the range of 1.55–1.71 were prepared by solution blending method using ZrO_2 nanoparticles as composite fillers in polyvinyl alcohol substrate. Compared with pure polyvinyl alcohol resin, the hybrid resin exhibits significant enhanced mechanical properties. Sub-kilogram-scale preparation of highly aqueous dispersible ZrO_2 nanoparticles offers possibility for practical applications.

1. Introduction

In recent years, the application of nanomaterials in new optical resins and electronic devices has received increasing attention [1–5]. A wide variety of nanomaterials, including carbon nanomaterial [6–8], semiconductor quantum dots (QDs) [9,10], rare-earth doped upconversion nanoparticles [11–13], metal oxide nanomaterials [14–16], have found great potential applications in the field of optoelectronics and beyond [17,18]. Among them, zirconia is a metal oxide having high melting point, high electrical resistivity, high refractive index (RI) and low coefficient of thermal expansion [19]. Due to the low cost, durability, and inactive chemical properties (not easily soluble in strong acid and alkali), ZrO_2 has been one of the most studied ceramic materials [20–22]. In recent years, along with the rapid development of nanoscience and nanotechnology, ZrO_2 nanoparticles (NPs) have been emerging as attractive materials for high RI nanocomposites [15,23,24]. The commercial available ZrO_2 NPs are usually mixed crystals of multiple phases and composed of aggregates with sizes of hundreds of nanometers to several micrometers. On one hand, producing phase-pure ZrO_2 NPs is important because phase purity defines their properties such as hardness, density and RI. Recently, our group reported the synthesis of aqueous ZrO_2 nanoparticles with a controllable crystalline phase (monoclinic and tetragonal) *via* the reaction of inorganic zirconium salt and sodium hydroxide in acid aqueous surrounding followed by hydrothermal process [23]. However, it is still challenging to realize the controllable preparation of pure cubic ZrO_2 NPs at low-cost and low energy-consumption.

One the other hand, the cost effective methods for controlling the dispersion of ZrO_2 NPs in polymeric hosts is a stumbling block to the large-scale production and commercialization of ZrO_2 based nanocomposites for advanced applications [15]. The commercial available ZrO_2 NPs are usually composed of particle aggregates with size of over hundreds of nanometers. A homogenous dispersion of the inorganic filler on the nanoscale is important in many applications, especially for

* Corresponding authors at: State Key Laboratory of Organic Inorganic Composites, Beijing University of Chemical Technology, Beijing 100029, China.
E-mail addresses: wangdan@mail.buct.edu.cn (D. Wang), puyuan@mail.buct.edu.cn (Y. Pu).
[1] These authors contributed equally to this work.

https://doi.org/10.1016/j.apsusc.2019.06.187
Received 21 March 2019; Received in revised form 16 June 2019; Accepted 18 June 2019
Available online 19 June 2019
0169-4332/

optical and optoelectronic devices in which the light transmission plays the critical role [11,15,23]. For instance, transparent hybrid optical resins with tunable refractive index using ZrO_2 NPs as fillers are highly required for advanced glasses and encapsulation [15,23]. Therefore, the issues related to scale-up, cost and compatibility of functional NPs must be considered at an earlier stage of development. The proper surface treatment of nanoparticles is the key to solving the problems of dispersion and compatibility.

Nowadays, the mixture of NaOH and H_2O_2, known as alkaline hydrogen peroxide (AHP), has been used as an effective surface treatment for commercial crystalline TiO_2 [25,26]. The AHP treated TiO_2 NPs had significantly enhanced visible-light photocatalytic degradation of dye contaminants compared to untreated TiO_2 NPs [26]. The AHP treatment as a pulping and bleaching method was originally used in papermaking industry [27], and also was used for biomass pretreatment [28–30]. In addition to the TiO_2 NPs related articles mentioned above, this method is rarely reported for the treatment of other NPs. The AHP treated TiO_2 NPs has a large number of hydroxyl groups on the surface to form a uniform and stable aqueous phase nanodispersion. Therefore, with the previous applications of the AHP method, it is worthwhile to try to prepare ZrO_2 nanodispersion on a large scale by the AHP method. At the same time, it should be pointed out that although the ZrO_2 NPs and TiO_2 NPs are both treated by the AHP treatment, the formation mechanism is different. The main reason is that TiO_2 NPs will dissolve in the AHP solution [25], but ZrO_2 NPs will not dissolve. The AHP treatment only can change the surface properties of ZrO_2 NPs. Therefore, the quality of ZrO_2 NPs before and after AHP treatment is not changed much, even if there is a loss, it is produced during the washing process. Therefore, the AHP method is more suitable for treating ZrO_2 NPs than TiO_2 NPs.

Herein, we propose a method for the synthesis of highly dispersible cubic phase ZrO_2 NPs by hydrothermal process coupled with AHP treatment. The agglomerated ZrO_2 NPs treated by the mixture of NaOH and H_2O_2 are highly dispersible in aqueous solution and can be prepared at sub-kilogram-scale in one batch reaction. The as-prepared cubic-ZrO_2 aqueous nanodispersion can be used to prepare thin composite films with high refractive index, and as filler in polymers to enhance optical and mechanical properties, which are both discussed in detail in our study.

2. Materials and methods

2.1. Materials

Deionized water used in this study was purified by a water purification system (Smart-S30, Hitech). Sodium hydroxide (NaOH), zirconium (IV) carbonate basic (ZCB, > 40 wt% ZrO_2), ethanol (ET), hydrogen peroxide (H_2O_2, 30%), nitric acid, methanol (MT), ethylene glycol (EG), glycerol (VG), and dimethyl sulfoxide (DMSO) were purchased from Aladdin Biochemical Technology Co., Ltd. (Shanghai, China). Polyvinyl alcohol (PVA) with a degree of polymerization of 1750 ± 50 and a saponification degree of 98–99% was bought from Tianjin Fuchen Chemical Reagents Factory. Commercialized ZrO_2 nanopowder was purchased from Sigma-Aldrich (544760, < 100 nm particle size). All the chemical reagents used in this work were analytically pure and were used without further purification.

2.2. Preparation of zirconia aqueous nanodispersion

A two-step procedure is applied in this work to synthesize the ZrO_2 aqueous nanodispersion. A slurry of ZrO_2 was first obtained from a hydrothermal process under extreme alkaline condition. The as-prepared slurry was then treated with AHP treatment to allow the growth of hydroxyl groups on ZrO_2 NPs surface. The representative preparation procedure of the whole experiment is depicted as in Scheme 1. First, the growth of $-Zr-O-Zr-$ networks from hydrolysis and condensation reaction of ZCB in the alkaline environment of pH = 13. This step ZrO_2 NPs had been produced, but the agglomeration degree of ZrO_2 NPs is serious. Second, the perhydroxyl anion (HOO^-) produced by H_2O_2 promoted the growth of ZrO_2 NPs surface hydroxyl groups in alkaline environment [26]. Later, the structure of Zr-O-Na could be exchanged by H^+ and to form Zr-OH bonds in the acid environment [25].

Typically, 20 g of NaOH was dissolved in 40 mL of deionized water at room temperature. Then 20 g of ZCB along with the as-prepared sodium hydroxide solution was transferred into a hydrothermal reactor. The reactor was heated at 110 °C for 6 h to form ZrO_2 crystal structure. At the same time, we also studied the influencing factors such as reaction temperature, reaction time, and the ratio of Na (mol)/carbonate (mol). The AHP treatment with different NaOH and H_2O_2 concentration gradients were applied to the ZrO_2 slurry which mentioned before. For the optimum condition, 85 mL of deionized water was added to the as-prepared ZrO_2 slurry to achieve the NaOH concentration of 4 M. Under vigorous stirring and a temperature of 50 °C, 5.1 mL of H_2O_2 (0.4 M) was added dropwise into the mixture. After 5 h of reaction, the mixture was centrifuged to remove the excess alkane solution. Subsequently, the ZrO_2 precipitate was rinsed with deionized water to remove as much alkane as possible. Finally, aqueous nitric acid (1.5 M) was added to the rinsed precipitation to form a solution which pH value was 1.0. A transparent and stable colloid of ZrO_2 NPs can be obtained after stirring. The yield of AHP treatment for zirconia nanoparticles is about 58.4%. The main mass loss during two-step reaction was mainly happening during the deionized water washing steps, which a portion of ZrO_2 NPs were dispersed in the water and taken away. The dosage of all chemical reagents can be amplified with the same magnification for large-scale manufacturing of ZrO_2 aqueous dispersion. However, when considering mass transfer and heating transfer during the reaction, stirring throughout the reaction should be comparatively stronger when the producing scale is significantly larger.

2.3. Preparation of transparent PVA/ZrO_2 nanocomposite film

The PVA/ZrO_2 nanocomposite films with different solid contents were prepared by simple mixing of PVA with the as-prepared aqueous cubic-ZrO_2 nanodispersion. Typically, stirring while heating at 90 °C in deionized water can dissolve PVA within 1 h. Then, to get a solid content of PVA/ZrO_2 mixtures with gradient, different amount of ZrO_2 aqueous dispersions were added into PVA - after which the mixture was sonicated for 5 min to generate a homogeneous solution. Consequently, the as-prepared PVA/ZrO_2 solutions were coated on glass slide or silicon slide to form PVA/ZrO_2 nanocomposite films by a spin-coating machine (Spin Coater, KW-4A). After heating and drying in a vacuum oven at 90 °C for 6 h for removing solvent. For the mechanical properties of PVA/ZrO_2 nanocomposite films, we prepare splines according to international standards (ISO 527-3:1995, IDT). Specifically, an aqueous solution of the composite having a solid content of 20% by weight (contains ZrO_2 and PVA) was coated on a PET substrate and then heated at 50 °C in a vacuum oven for 5 h. Finally, the formed PVA/ZrO_2 nanocomposite film was peeled off from the PET substrate and cut into the shape of a standard spline for testing.

2.4. Characterization

The transmission electron microscope (TEM) images of the ZrO_2 NPs were taken using a Hitachi HT-7700. Zeta potential and size distribution of the ZrO_2 NPs were determined by DLS (Nano ZS90, Malvern). The X-ray diffraction (XRD) patterns of the samples were measured by an XRD-6000 diffractometer (Shimadzu Inc.). The Raman spectrum of the samples was measured by a micro-Raman spectroscopy system (Excitation wavelength 514 nm, Renishaw inVia). A PerkinElmer spectrum GX FTIR spectroscopy system was used to record the Fourier transform infrared spectroscopy (FTIR) spectra of solid samples. The X-ray photoelectron spectroscopy (XPS) measurements were carried out

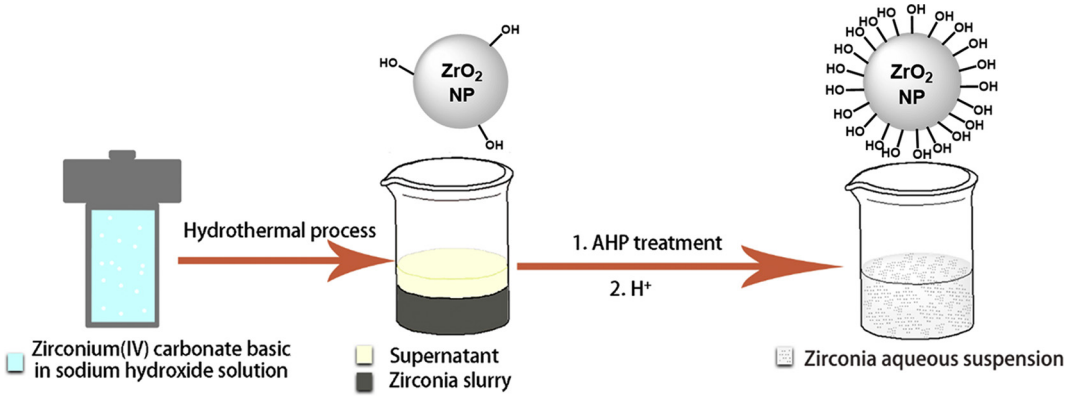

Scheme 1. Schematic diagram of the routes for the preparation of highly dispersible ZrO_2 NPs.

by using a 250XI X-ray photoelectron spectrometer (Shimadzu Inc.). Thermogravimetric analysis (TGA) and differential scanning calorimeter (DSC) were performed by using a Q50 TGA from TA Instruments. Surface morphology of the hybrid films were examined by using a scanning electron microscope (SEM, Hitachi S4800). The RI of the films was measured by an ellipsometer (UVSEL, HORIBA, France) in the range of 250 nm to 800 nm. UV–vis absorbance and transmittance results were tested with a Varian Cary 50 spectrophotometer. The dispersibility of ZrO_2 NPs could be quantitatively evaluated by the following equation [31]:

$$D_{24}\% = \frac{T_0}{T_{24}} \times 100\%$$

where $D_{24}\%$ was the transmittance change of the dispersion, T_0 and T_{24} were the transmittances of initial ZrO_2 nanodispersion and the ZrO_2 nanodispersion after standing for 24 h, respectively [26]. The higher the value of $D_{24}\%$, the better of the dispersibility of ZrO_2 nanodispersion.

3. Results and discussion

The crystal form change of ZrO_2 NPs under different hydrothermal conditions was studied. Firstly, the influencing factor of this work is the ratio of NaOH to ZCB (Na(mol)/carbonate(mol), abbreviated as Na/C). Fig. 1a shows the XRD patterns of the samples of the ZrO_2 NPs by the hydrothermal method under the radio of Na/C from 0.77 to 3.83. It can be obviously observed that all of the diffraction peak positions of the samples were in good agreement with the International Center for Diffraction Data (ICDD) for cubic ZrO_2 crystal (PDF: 49-1642). The diffraction peaks of ZrO_2 at 30.12°, 34.96°, 50.22°, and 59.74°, which correspond to the crystal planes of (111), (200), (220), and (311) respectively. It can be found that as the ratio of Na/C decreases, the grain size of the ZrO_2 NPs becomes larger according to Scherrer's equation. The Raman scattering spectrum reveals the characteristic peak of cubic ZrO_2 at 500–600 cm^{-1}, proving another evidence for the formation of cubic ZrO_2 (Fig. 1b) [32].

When the molar ratio of Na/C reaches 0.38, the ZrO_2 NPs are not in pure cubic phase, and some ZrO_2 NPs are in monoclinic phase. As shown in Fig. 1c, the diffraction peaks at 24.16°, 24.63°, 28.34°, and 31.48°, which belonged to monoclinic phase ZrO_2 (PDF:80-0966). However, it is difficult for distinguishing cubic and tetragonal phases of ZrO_2 NPs according to PDF 49-1642 and PDF 88-1007. To make a distinction between tetragonal and cubic phases, Raman spectroscopy was used as an additional technique (Fig. 1d). From the Raman spectrum, it can be found that the crystal phase of ZrO_2 is a mixture of cubic phase and monoclinic phase. The strong peaks at 180, 340, 380, and 480 cm^{-1} were assigned to the monoclinic phase [23] and the broad band in the range of 500–600 cm^{-1} can be observed as the characteristic peaks of cubic ZrO_2 [23,33]. Since a mixed phases material may undergo phase transformation in the subsequent process, some problems caused by changes in volume and shape during the phase change [34–37]. Simultaneously the cubic phase ZrO_2 has the highest symmetry and lowest aspect ratio among three phases, so it is desirable to prepare uniformly dispersed cubic-ZrO_2 nanodispersion. Therefore, in combination with the previous experiments, it is crucial to increase the ratio of the Na/C to a reasonable range.

It can be found from Fig. 2a that as the reaction temperature increases from 110 to 200 °C, the phase of zirconia does not change and always is cubic phase. But as the temperature increases, the grain size of ZrO_2 NPs becomes large. At the same time, the Raman spectrum in Fig. 2b also proves this. It can be seen from Fig. 2c–d that the time of the reaction has no significant effect on the crystal phase and the particle size of the ZrO_2 NPs. Therefore, the preparation of highly crystalline cubic-ZrO_2 NPs can be prepared just in a short time and at a lower reaction temperature than general approach [23]. This is important for whether it can perform large-scale amplification experiments. Fig. S1 shows the change of ZrO_2 NPs phase at different calcination temperatures. The phase of ZrO_2 NPs can be analyzed by XRD and Raman to remain unchanged as cubic phase under the condition of room temperature to 500 °C. As the calcination temperature increases, the ZrO_2 NPs changes from a single cubic phase to a mixed crystal phase of a cubic phase and a monoclinic phase at 700 °C. This puts new demands on the ZrO_2 NPs prepared by this method. If the temperature exceeds 700 °C in the application process, the volume change caused by the crystal phase change of NPs needs to be considered. In this case, it is necessary to dope some other oxides in ZrO_2 NPs to stabilize the crystal phase, such as calcium oxide [38,39], cerium oxide [40–42], and yttrium oxide [43,44], *etc*.

The DLS-based size distribution of the ZrO_2 NPs sample (Na/C = 3.06, 110 °C, 6 h) was shown in Fig. S2. From the results of the particle size, it can be found that the distribution was narrow, but the degree of particle agglomeration was serious. Then this solid sample was added to the water, and it is completely precipitated at the bottom for about 10 min, and cannot be uniformly dispersed in the water. Large areas of agglomeration had also been observed by TEM (Fig. S3), mainly due to the excessive surface energy of the nanoparticles. The agglomeration of ZrO_2 NPs is what the researchers want to avoid. In principle, to make the ZrO_2 NPs disperse uniformly and stably in water, generally two steps are required. One is to give a force to separate the agglomerated ZrO_2 NPs; the other is to give a stable repulsion force on the surface of the disassembled nanoparticles to make them stably dispersed. The repulsion force generally has two types of steric effect and electrostatic effect. The steric effect is generally achieved by grafting various coordination groups on the surface, such as fatty acids and silane coupling agents [15,32]. In the method used in this paper, no coordination group is used, and the stability of the nanoparticles is mainly due to electrostatic effect. The particle size distribution and colloidal stability of AHP-treated ZrO_2 were investigated by DLS and

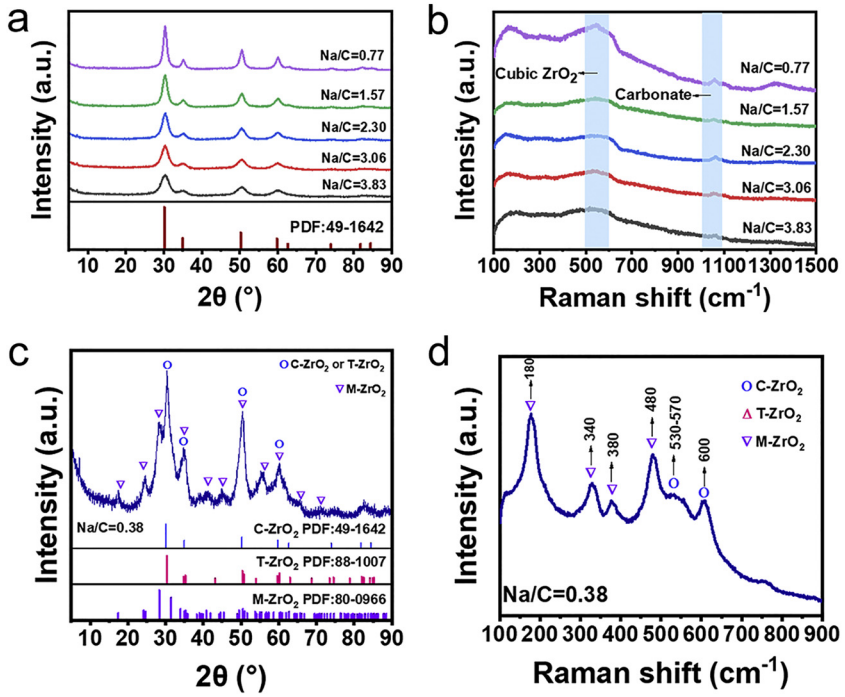

Fig. 1. (a) XRD patterns of the ZrO_2 NPs under the ratio of the Na/C from 0.77 to 3.83; (b) Raman spectrums of the ZrO_2 NPs under the ratio of the Na/C from 0.77 to 3.83; (c) XRD patterns of the ZrO_2 NPs under the ratio of the Na/C is 0.38. (d) Raman spectrum of the ZrO_2 NPs under the ratio of the Na/C is 0.38.

UV–vis transmittance change (D_{24}%). Fig. 3a–d show the performance of AHP-treated ZrO_2 under functions of NaOH concentration and H_2O_2 concentration. As shown in Fig. 3a, the Z-average particle size decreased first and then increased with an increase of NaOH concentration up to 10 M. The colloidal stability increased dramatically first then decreased with an increase of NaOH concentration. The results found that the concentration of NaOH is too low or too high, which will cause serious agglomeration of ZrO_2 NPs. ZrO_2 NPs can form a stable dispersion because during the pickling process, H ions form an electric double layer with the surface of the zirconia. The whole ZrO_2 NPs are positively charged, and the repulsive action of the charge forms a stable dispersion. Therefore, the degree of dispersion of zirconia should also be determined by the concentration of H ions on the surface, which depending on the degree of hydroxylation of the zirconia surface [45]. The hydroxylation of the surface of the ZrO_2 NPs depends on the degree of contact of the surface of the zirconia with the H_2O_2 and the degree of reaction. The reaction of the surface of ZrO_2 NPs and H_2O_2 is achieved under alkaline conditions, in which case the ZrO_2 surface is negatively

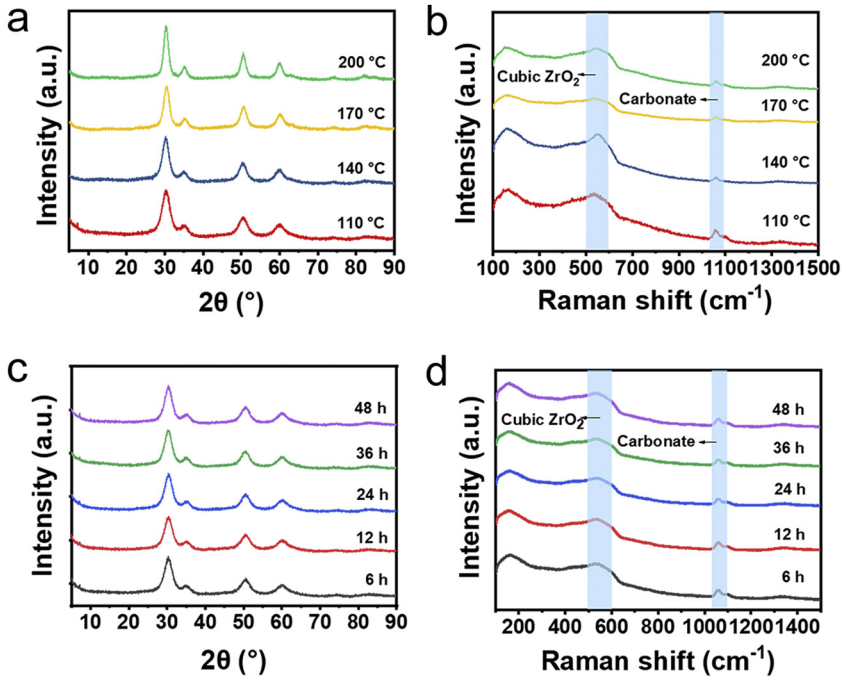

Fig. 2. (a) XRD patterns of the ZrO_2 NPs under temperatures from 110 °C to 200 °C; (b) Raman spectrums of the ZrO_2 NPs under temperatures from 110 °C to 200 °C; (c) XRD patterns of the ZrO_2 NPs under times from 6 to 48 h. (d) Raman spectrum of the ZrO_2 NPs under times from 6 to 48 h.

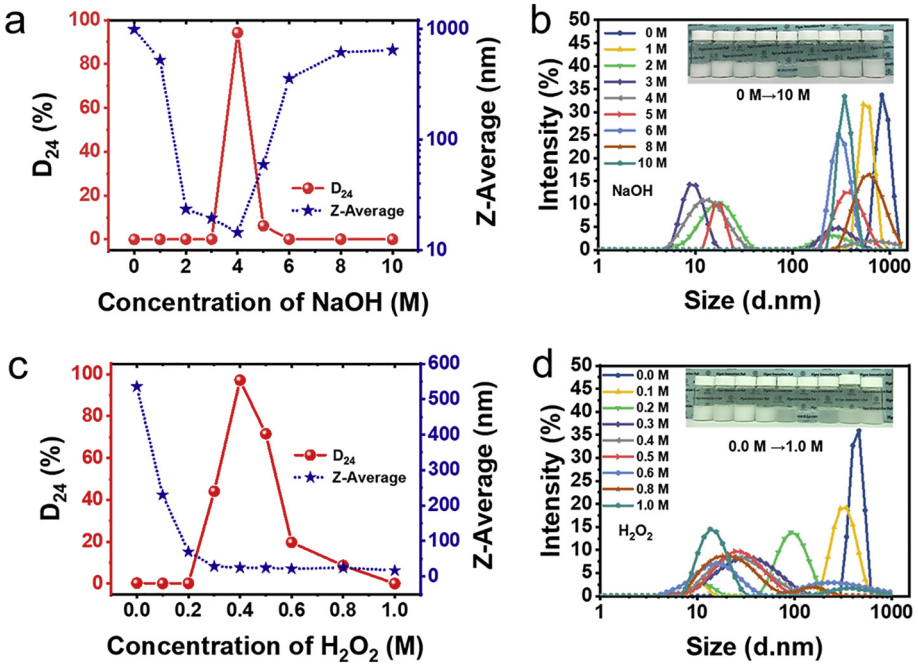

Fig. 3. Z-average particle size and colloidal stability (D_{24}) of ZrO_2 NPs prepared with different concentrations of (a) NaOH and (c) H_2O_2. DLS-based size distribution of ZrO_2 NPs prepared with different concentrations of (b) NaOH and (d) H_2O_2.

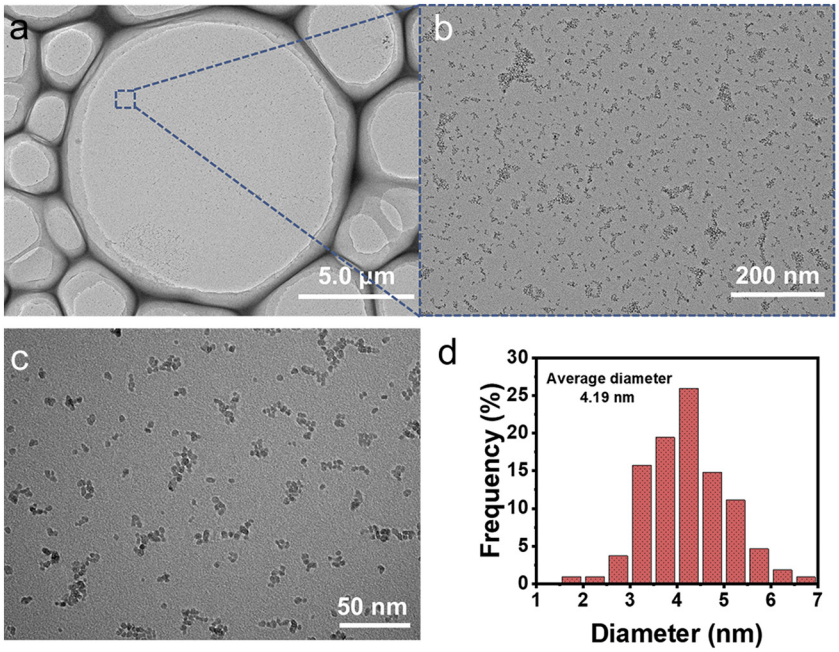

Fig. 4. TEM images for (a, b, c) the AHP-treated ZrO_2 NPs. The particle size distribution (d) for the AHP-treated ZrO_2 NPs.

charged. When the alkalinity is enhanced, the charge repulsion is also increased. Although the ZrO_2 NPs are still in agglomerated state, the chance of contact of the H_2O_2 with the surface of the zirconia is increased, and the hydroxylation rate is also increased. As the concentration of NaOH increases continuously, the amount of ions in the solution increases greatly, which in turn hinders the contact of H_2O_2 with the surface of the zirconia. Based on the above results, 4 M NaOH was chosen as the optimum concentration. The results on the effect of H_2O_2 concentration on the performance of AHP-treated ZrO_2 are shown in Fig. 3c. The Z-average particle size decreased quickly with an increase of H_2O_2 concentration up to 1 M. When the concentration of H_2O_2 is 0.3 M, the Z-average value of ZrO_2 NPs has been reduced to 28.20 nm, and with the further increase of H_2O_2 concentration, the Z-average value has not decreased correspondingly, indicating that the near saturation of the solution affected the contact between the H_2O_2 and the ZrO_2 surface. The colloidal stability increased dramatically first then decreased with an increase of H_2O_2 concentration. This means that if there are some residual hydrogen peroxide molecules, it will also affect the stability of the ZrO_2 NPs dispersion. The Z-average value results are shown in Table S1 and Table S2.

Fig. 4a–c shows the TEM images of AHP-treated ZrO_2. As can be seen, ZrO_2 NPs were monodisperse and spheroidal in a wide area, indicating that AHP treatment can be re-modified with ZrO_2 NPs surface. This is different from the previous formation mechanism of this AHP

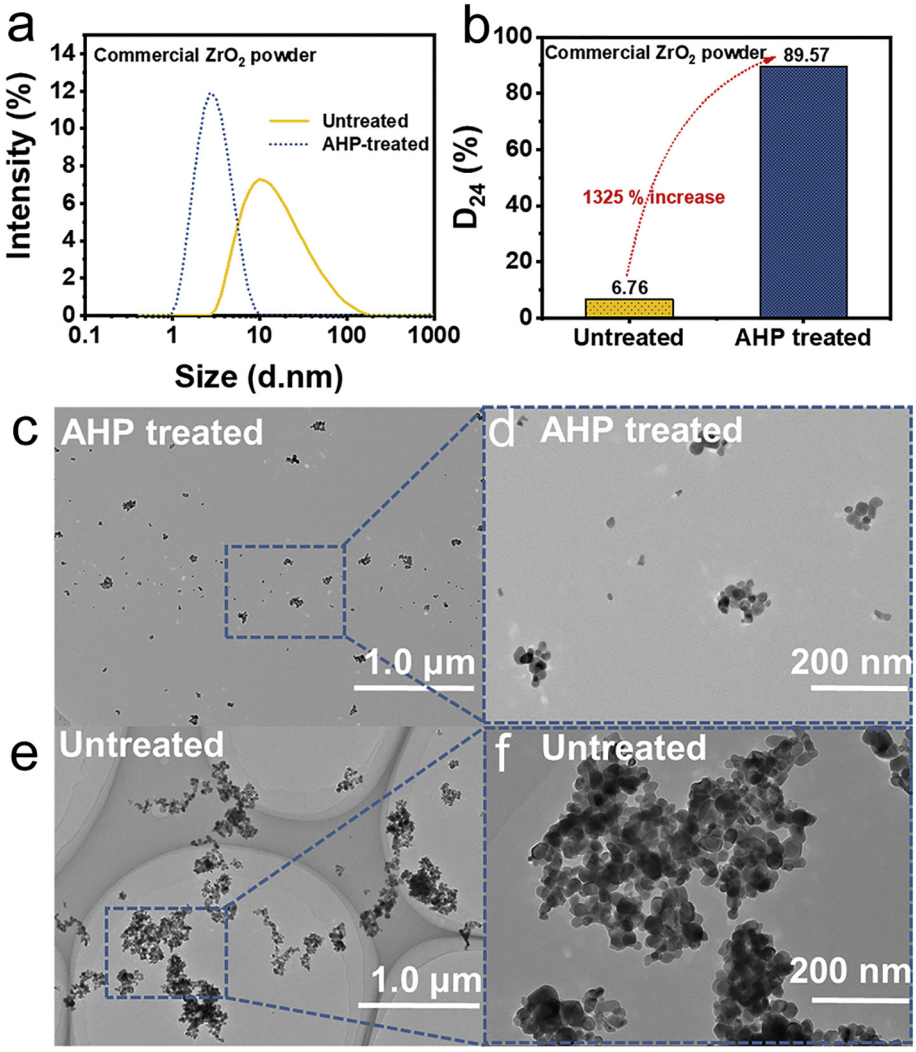

Fig. 5. (a) DLS-based size distribution and (b) colloidal stability of the commercial ZrO_2 NPs before and after AHP treatment. TEM images for (c, d) the AHP-treated ZrO_2 NPs and (e, f) untreated ZrO_2 NPs.

treatment for TiO_2. ZrO_2 is not easy to dissolve in strong acid and alkali compared to TiO_2, even in a strongly oxidizing alkaline environment in the presence of H_2O_2. The untreated ZrO_2 NPs showed serious agglomeration and the average diameter was determined to be about 600 nm (Fig. S3). Nevertheless, AHP-treated ZrO_2 well-separated primary particles with an average size of 4.19 nm (Fig. 4d). This average diameter size is also matched to the calculated crystalline sizes in the XRD result. It is worth mentioning that the surface of the agglomerated ZrO_2 NPs after hydrothermal are rich with carbonate groups, which is the reason why the single ZrO_2 NP do not grow up after agglomeration, and it is also the reason why we can easily obtain sub-kilogram-scale synthesis of highly dispersible ZrO_2 NPs by AHP treatment. Besides, the water-dispersible AHP-treated ZrO_2 could be stable over months without any surface modifier. This behavior could be considered to electrostatic repulsion between nanoparticles [23,46–48], which results from a high surface charge of AHP-treated ZrO_2 in an acidic environment. The zeta potential of the AHP-treated ZrO_2 nanodispersion was 34.2 mV. At the same time, it was observed that the powders obtained by drying the acidic AHP-treated zirconia aqueous phase dispersion at normal temperature ($< 100\,^{\circ}C$) can be dispersed again in water (Fig. S4).

The AHP treatment experiment was also carried out on the purchased commercial ZrO_2 powder. The reaction condition is optimal for NaOH concentration (4 M) and H_2O_2 concentration (0.4 M). The commercial ZrO_2 powder treated by AHP treatment can be acid washed to form a transparent nanodispersion. From the DLS particle size distribution in the Fig. 5a, it was obvious observed that the ZrO_2 powder after AHP treatment was significantly smaller than the untreated ZrO_2 powder. It can be seen from the result of D_{24}% that the dispersion stability of the ZrO_2 powder treated by AHP treatment was significantly higher than that of the untreated sample (Fig. 5b). From the comparison of TEM images (Fig. 5c–f), it can be found that the agglomeration of the AHP-treated ZrO_2 is greatly reduced. The photographs of Fig. S5 separately recorded the settlement process of the AHP-treated ZrO_2 nanodispersion (1 wt%) and the untreated dispersion (1 wt%) at different times from 1 h to 24 h, showed the high stability of the ZrO_2 nanodispersion treated by the AHP treatment intuitively. This proves that the AHP treatment method is still applicable to the general commercial nanopowder, which shows that the AHP method has universality.

As shown in Fig. 6a, it can be seen from the XRD results that the crystal phase of ZrO_2 NPs at different stages of treatment had not changed. The crystal phase of ZrO_2 NPs is cubic phase, which means that the AHP treatment does not change the internal crystal phase, only the surface of ZrO_2 NPs is treated. At the same time, it was found that there was a small amount of characteristic peak of $NaNO_3$ (PDF: 85-0850) in the sample after acid treatment if the sample is not adequately cleaned by water (Fig. S6). Sodium ion comes from sodium hydroxide in AHP treatment. Since sodium ions are replaced by hydrogen ions

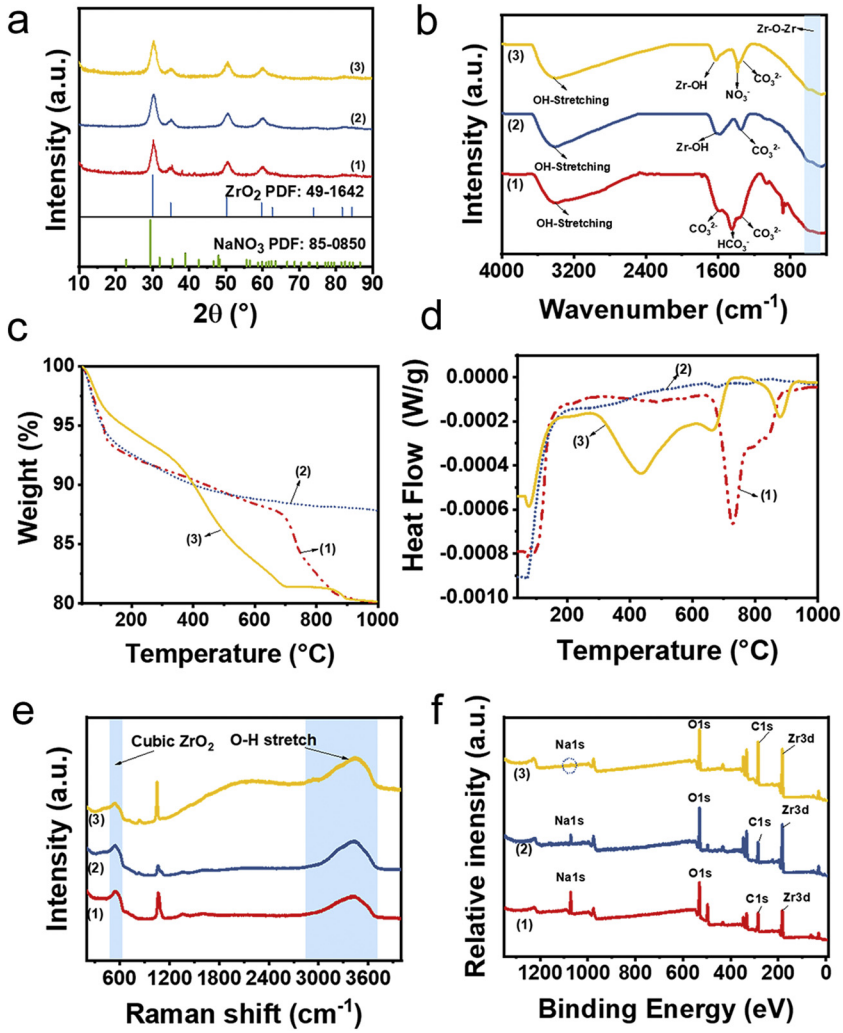

Fig. 6. XRD spectra (a) of ZrO_2 powders at different stages. FTIR spectra (b) of ZrO_2 powders at different stages. Raman spectra (c) of ZrO_2 powders at different stages. XPS spectra (d) of ZrO_2 powders at different stages. Three stages of ZrO_2 powders: (1) untreated ZrO_2, (2) AHP-treated ZrO_2 before acid treatment, and (3) AHP-treated ZrO_2 after acid treatment.

during the acid treatment process, the sodium ions in the sample after pickling can be easily removed from the surface of ZrO_2 NPs, and the XRD results of the ZrO_2 NPs after washing is substantially free of sodium nitrate. The presence of sodium nitrate has a negative effect on the smoothness of the composite film and the transparency of the dispersion, so the cleaning process is necessary. Fig. 6b shows the FTIR spectra of ZrO_2 powders at different stages. The untreated ZrO_2 NPs surface has many carbonate groups. The 1607, 1442, and 1350 cm^{-1} can be observed as the carbonate coordinated to the ZrO_2 NPs surface [49]. After the AHP treatment before acid treatment, new bands appeared at 1572 cm^{-1} can be considered as the bending of OH [50]. For the AHP treatment after acid treatment, the peak appeared at 1627 cm^{-1} can be considered as the bending of Zr-OH [51]. The small spike at 1383 cm^{-1} can be considered as the nitrate coordinated to the ZrO_2 NPs surface [52–54]. The source of nitrate is derived from the nitric acid used for acid treatment. The hydroxyl groups on the surface of AHP-treated ZrO_2 are significantly increased compare to untreated ZrO_2. Fig. 6c–d shows the TGA and DSC curves of the ZrO_2 powders at different stages. The weight loss curves of the unmodified ZrO_2 NPs and the AHP-treated ZrO_2 NPs before acid treatment are basically the same from 40 °C to 500 °C. However, the unmodified sample has a distinct exothermic peak at 700 °C, presumably caused by the decomposition of the carbonate groups. The AHP-treated ZrO_2 NPs after acid treatment have an exothermic peak at 450 °C and 690 °C due to the large amount of surface hydroxyl groups. Fig. 6e shows Raman spectra of ZrO_2 NPs at different stages exhibited a similar broad band in the range of 500–600 cm^{-1} for cubic phase. The Raman spectra is processed and normalized for semi-quantitative analysis based on the peak of 542 cm^{-1}. The increased -OH on the surface of AHP-treated ZrO_2 were confirmed by the results where the strong and broad absorption band in the range of 3000–3600 cm^{-1} were attributed to -OH on the surface of ZrO_2 [55]. The intensity of the peak at 1100 cm^{-1} is significantly increased after acid treatment, and the peak is considered as the carbonate and nitrate. It is speculated that the -OH on the surface of ZrO_2 NPs increase, and the carbonate or nitrate coordinated to the -OH is also more, which is the main cause of the change in peak's intensity. This proves on the side that the surface hydroxyl groups of the ZrO_2 NPs are increased after acid treatment. Fig. 6f shows XPS survey spectra of the surface of the ZrO_2 powders at different stages. It can be seen that the elemental composition among untreated ZrO_2, AHP-treated ZrO_2 before and after acid treatment are almost the same, as shown in Table S3. The element Na was decreased in AHP-treated ZrO_2 after acid treatment. This could be attributed to the H^+ replace a part of Na^+ [26]. Therefore, Na^+ can be easily removed from the particle system during the cleaning process. Another reason is that the addition of nitric acid causes the pH of the system to fall less than the isoelectric point of ZrO_2 so that the surface of the ZrO_2 is positively charged, and the positive ions such as Na^+ particles are easily detached from the surface of the

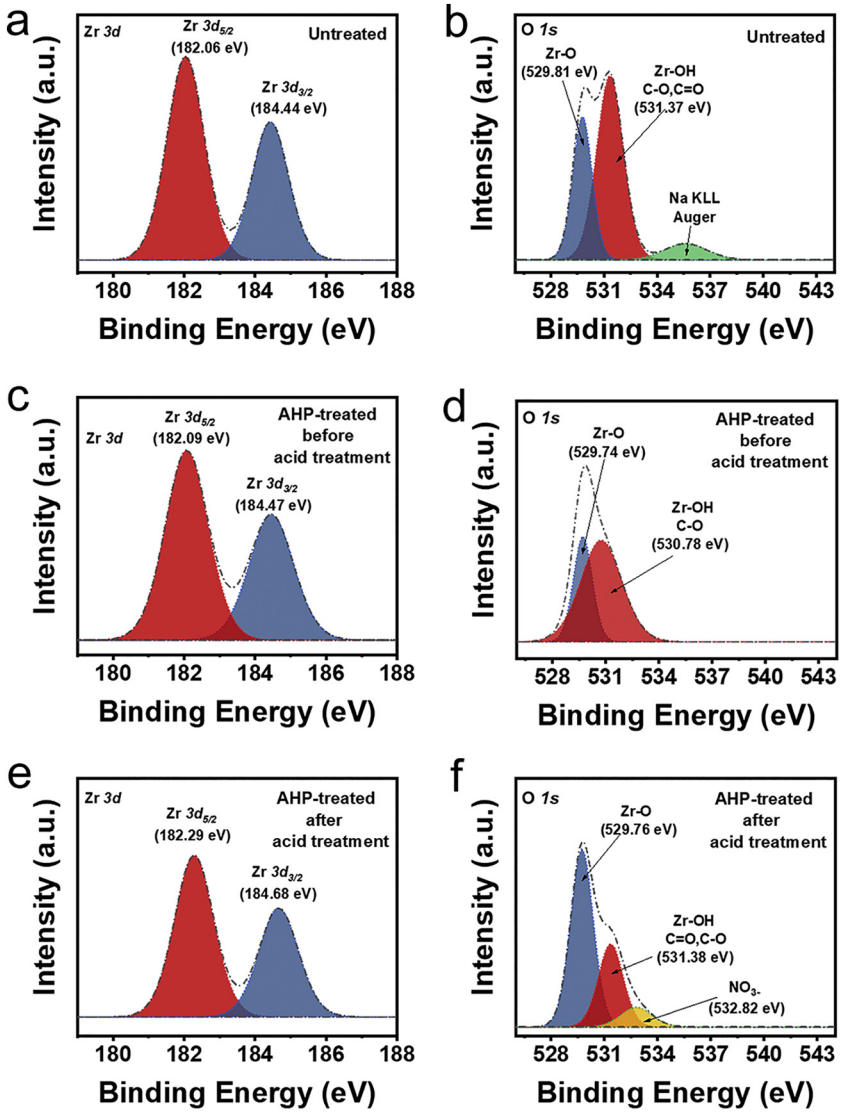

Fig. 7. XPS core level spectra of samples (a, c, e) Zr (3d) and (b, d, f) O (1s).

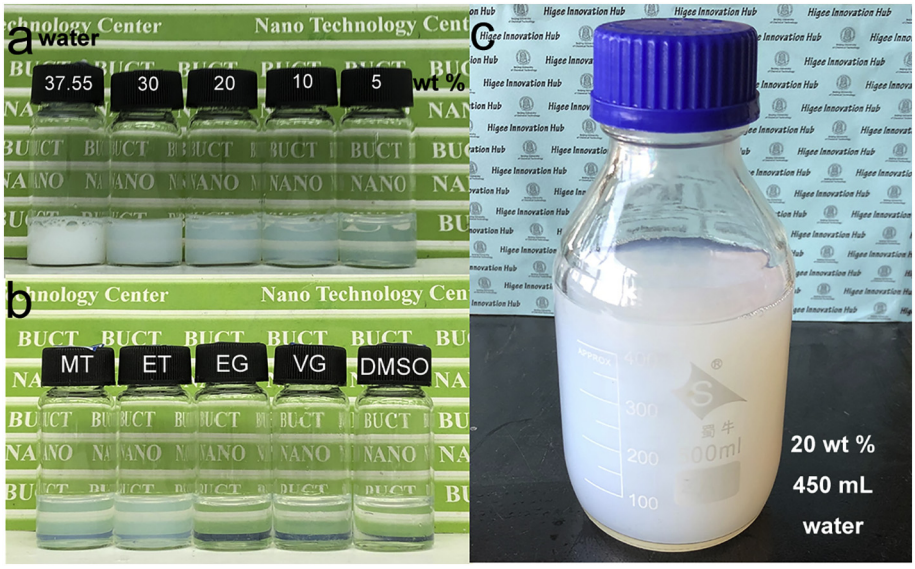

Fig. 8. (a) Photographs of aqueous ZrO_2 NPs with different solid contents from 5 wt% to 37.55 wt%, and (b) ZrO_2 NPs with different solvent and the same solid content of 5 wt%. (c) A photograph of 450 mL aqueous cubic-ZrO_2 nanodispersions with a solid content of 20 wt%.

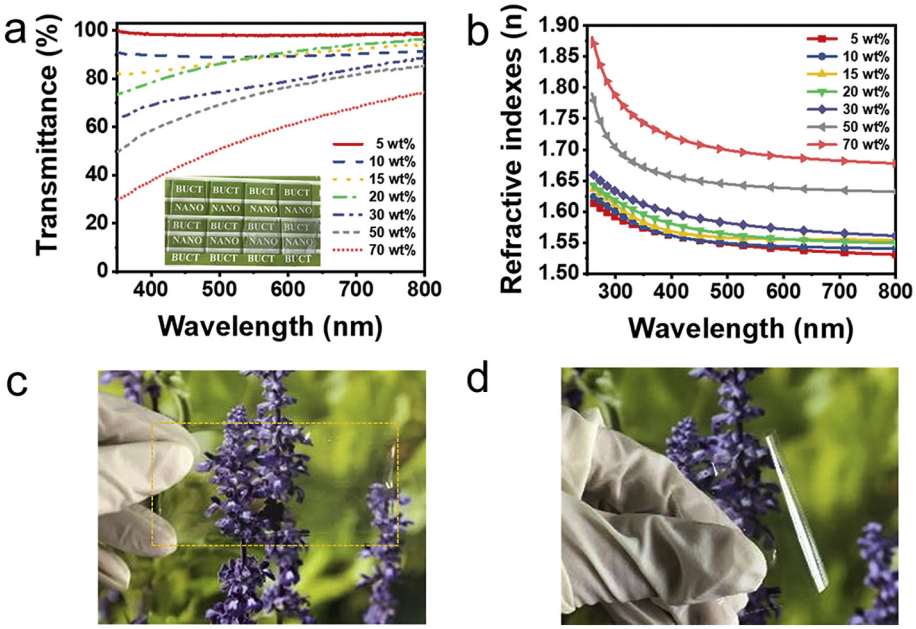

Fig. 9. The transmittance spectra (a) and the RI (b) of PVA/ZrO_2 hybrid films with different ZrO_2 contents prepared from transparent aqueous cubic-ZrO_2 nanodispersions. Digital photographs (c–d) of PVA/ZrO_2 hybrid films.

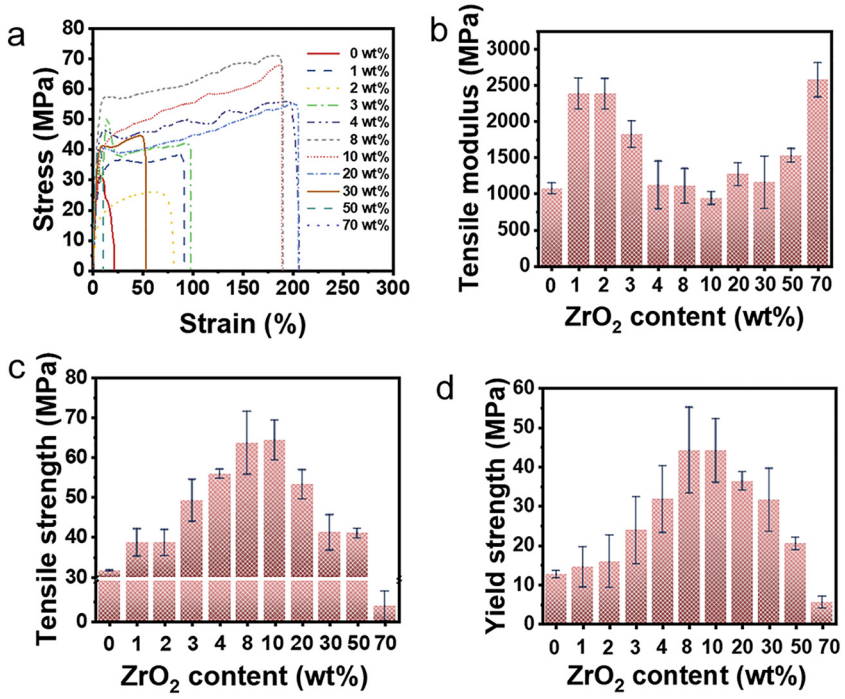

Fig. 10. Stress-strain curves (a) of PVA/ZrO_2 hybrid films. Tensile modulus testing results (b), tensile strength result (c), and yield strength result (d) of the samples.

ZrO_2. In the corresponding reason, carbonate ions are easily adsorbed on the surface of ZrO_2, which is why the ions such as carbonate and nitrate on the surface of ZrO_2 after AHP treatment increase.

Fig. 7(a, c, e), (b, d, f) shows the XPS spectra of the Zr *3d* and O *1s* core levels of the ZrO_2 powders at different stages, respectively. In previous reports, Basahel [56] reported that the peaks located at 181.3 and 183.8 eV are considered to the Zr *3d* components, Zr $3d_{5/2}$ and Zr $3d_{3/2}$. The binding energy of O *1s* of ZrO_2 NPs is located at 530.1 eV. Kawasaki [57] measured that Zr *3d* components, Zr $3d_{5/2}$ and Zr $3d_{3/2}$ for cubic phase ZrO_2 NPs can be observed at 182.0 and 184.4 eV, respectively. The untreated ZrO_2, AHP-treated ZrO_2 before and after acid treatment appeared at about 182 and 184 eV and Zr *3d* components observed in this study are in consistent with values reported in the literature. Navio et al. [58] reported the oxygen species of ZrO_2 and oxygen species of Zr-OH, whose binding energy is in the range of 529.8 to 530.3 and 530.9 to 532.2 eV, respectively. As shown in Fig. 7b, the O *1s* broad peaks deconvolution indicated the peaks at 529.81, 531.37, and 535.87 eV could correspond to Zr—O in ZrO_2, Zr-OH, and Na KLL Auger of the untreated ZrO_2 NPs, respectively. The speculation of Na KLL Auger comes from the standard XPS spectrum of sodium bicarbonate on the official website of Thermo Scientific. Among them, the peak at 531.37 eV could correspond to mixture of Zr-OH, C—O, and C═O. Because it was also found in Fig. S7, the C *1s* broad peaks deconvolution indicated the peaks at 284.82, 286.05, and 289.42 eV could correspond

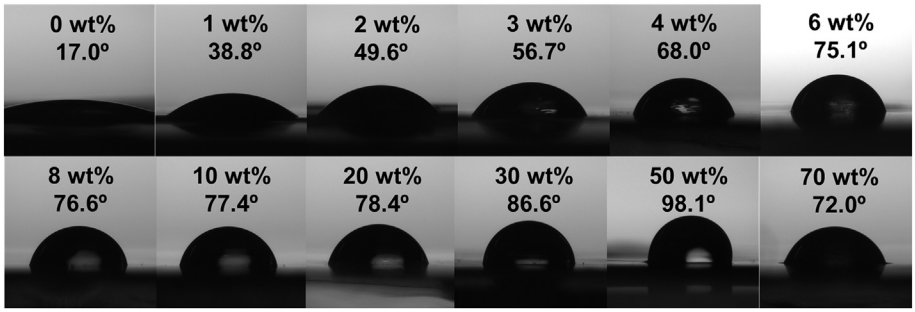

Fig. 11. Relationship between contact angle and the amount of zirconia added in the PVA resin.

to C—C, C—O, and O-C = O the untreated ZrO_2 NPs, respectively. Figs. 7d and S8 show that no peak of the O-C = O group was found, thus indicating that the free carbonic acid group was substantially washed away and peaks at 530.78 correspond to mixture of Zr-OH and C—O. As shown in Figs. 7f and S9, the peak deconvolution indicated that the peaks at 529.76, 531.38, and 532.82 eV could correspond to Zr—O in ZrO_2, the hydroxyl group and nitrate group, respectively. It is clear that the changes of the ZrO_2 surface groups before and after AHP treatment by XPS result.

Fig. 8 presents the digital pictures of 5, 10, 20, 30, 37.55 wt% transparent aqueous cubic-ZrO_2 nanodispersions. The transparency of the aqueous cubic-ZrO_2 nanodispersion decreased with increasing weight content, and at the same time it was found that the maximum weight content which can be stably dispersed at 37.55 wt% (Fig. S10). This aqueous solution exhibited a uniform hydrodynamic size of 14.15 ± 5.834 nm and was stable for over six months without significant aggregates. Above this solid content, there will be sedimentation. Furthermore, the as-prepared ZrO_2 NPs could be easily dispersed in many solvents with high polarity including MT, ET, EG, VG and DMSO, forming stable and transparent nanodispersions with a solid content of 5 wt%. It can be seen from Figs. S11–S12 that the cubic-ZrO_2 nanodispersion of different solvents has a high transmittance in the visible light region and a high absorption rate in the ultraviolet light region. At the same time, 450 mL of aqueous cubic-ZrO_2 nanodispersions with a solid content of 20 wt% was also shown (Fig. 8c), which also shows this method can achieve large-scale synthesis.

Pharmaceutical grade PVA, unlike chemical grade PVA, is an extremely safe polymer organic substance with non-toxic to humans, no side effects, good biocompatibility, good film forming, and good mechanical properties [51,59,60]. It is widely used in ophthalmology, wound dressings and artificial joints, and is also used in polyvinyl alcohol film in medical films, artificial kidney films and the like. Due to the high RI of ZrO_2 [61] (n = 2.2), one of promising applications of ZrO_2 fillers is to make high RI composite polymers. PVA is very suitable as a matrix for aqueous cubic-ZrO_2 nanodispersion due to its good water solubility and film forming properties. Fig. 9a shows the transmittance spectra of nanocomposite films with different concentrations of ZrO_2 embedded in PVA. PVA films showed high transparency in the visible region with the content of ZrO_2 in the range of 0–20 wt%. With the increase of ZrO_2 content from 30 to 70 wt% in the hybrid films, the visible light transmittance in the range of 400–800 nm had a decrease. The RI of hybrid films with different ZrO_2 solid contents in the range of 250–800 nm were measured and the results are presented in Fig. 9b, in which the RI of the hybrid film is increased as the content of ZrO_2 increases. The high RI could reach 1.71 (500 nm) by increasing the corresponding mass fraction of ZrO_2 to 70%. Fig. 9c–d shows that a PVA/ZrO_2 nanocomposite film having a zirconia addition amount of 20% by weight has excellent transparency and bendability, and the thickness of the film is about 0.1 mm.

Fig. 10a shows the stress-strain curves for PVA/ZrO_2 nanocomposite films, whose solid content ranges from 0 wt% to 70 wt%. There is a significant increase in the toughness with the addition of AHP treated ZrO_2 NPs, where samples with 8 wt% ZrO_2 has the highest toughness. Also, when comparing to the pure PVA sample, the elongation percentage is significantly increased (about seven times greater when the solid content is 20 wt%). The addition of ZrO_2 NPs increases the optical properties and mechanical properties of the PVA/ZrO_2 nanocomposite film such as refractive index and toughness, which greatly expands the application of the nanocomposite film. Fig. 10b shows the tensile modulus, and the material is more flexible when the solid content is around 10 wt% and is more rigid when either the solid content is too high or too low. According to Fig. 10(c–d), samples with higher solid content are more ductile (under 10 wt%). It shows the addition of ZrO_2 NPs can significantly toughen the polymer matrix, and the sample with 10 wt% ZrO_2 has the best toughening effect and greatest tensile strength. Consequently, the tensile strength increased from 31.47 MPa to 67.77 MPa and the yield strength increased from 11.36 MPa to 41.31 MPa. When the solid content exceeds 10 wt%, the material then becomes more brittle is subjugated to sudden crack. The addition of ZrO_2 NPs causes stress concentration in the PVA matrix, which can cause the formation of silver streaks and absorb a certain deformation work. At the same time, if the amount of ZrO_2 NPs added is too large, the particles are too close and have developed macroscopic cracking, so the performance of the materials is rather reduced. Compared with previous work [62], the toughening effect is much greater in our work. The reason is that the grain size of the ZrO_2 NPs added in this work is much smaller than other work [62]. At the same time, the uniform dispersion of the AHP treated ZrO_2 NPs in the PVA mixed solution is also good, and we can find that the composite film in other literatures is not transparent [62]. This greater enhancement of mechanical properties should be giving credit to the homogeneity of ZrO_2 NPs in the PVA matrix.

The contact angle increases continuously from 17.0° to 98.1° when ZrO_2 content increases from 0 wt% to 50 wt%, indicating the incorporation of ZrO_2 NPs can enhance the hydrophobicity of the PVA matrix (Fig. 11). Notably, the nanocomposite film becomes hydrophobic when the solid content reaches 50 wt%, which shows the potential for preparing hydrophobic PVA films. When adding aqueous ZrO_2 NPs into the PVA matrix, hydroxyl groups on the polymer chains tend to form hydrogen bonds with hydroxyl groups on ZrO_2, which allows less free hydroxyl groups to form hydrogen bonds with water molecules. Thus, the film becomes more and more hydrophobic when adding a certain amount of ZrO_2. However, when there is too much ZrO_2 in the matrix, excess hydroxyl groups on ZrO_2 will start to bond with water and lower the hydrophobicity.

4. Conclusion

We reported a facile, repeatable and green method to synthesize highly transparent and stable cubic-ZrO_2 aqueous nanodispersion. The AHP treatment as a universal method is also can improve the performance of commercial ZrO_2 powder. Characterization methods in this work prove that an increase of surface hydroxyl groups on ZrO_2 facilitates the long-term stability of the aqueous nanodispersion. The as-

prepared cubic-ZrO_2 aqueous nanodispersion can be used to prepare hybrid films with PVA showed a high refractive index of 1.71 (500 nm). The highly transparent ZrO_2 NPs in water without any modification ligand is very promising for further applications in energy, optical coating, and biomedical fields.

Acknowledgments

We are grateful for financial support from National Key Research and Development Program of China (2017YFB0404302/2017YFB0404300).

Appendix A. Supplementary data

Supplementary data to this article can be found online at https://doi.org/10.1016/j.apsusc.2019.06.187.

References

[1] J. Zhu, J.-W. Lee, H. Lee, L. Xie, X. Pan, R.A. De Souza, C.-B. Eom, S.S. Nonnenmann, Probing vacancy behavior across complex oxide heterointerfaces, Sci. Adv. 5 (2019) 8467.
[2] M.M. Arafat, J.Y. Ong, A.S.M.A. Haseeb, Selectivity shifting behavior of Pd nanoparticles loaded zinc stannate/zinc oxide (Zn_2SnO_4/ZnO) nanowires sensors, Appl. Surf. Sci. 435 (2018) 928–936.
[3] M. Haming, T.T. Baby, S.K. Garlapati, B. Krause, H. Hahn, S. Dasgupta, L. Weinhardt, C. Heske, The effect of NaCl on room-temperature-processed indium oxide nanoparticle thin films for printed electronics, Appl. Surf. Sci. 396 (2017) 912–919.
[4] M. Xiao, S. Wang, S. Thaweesak, B. Luo, L. Wang, Tantalum (oxy)nitride: narrow bandgap photocatalysts for solar hydrogen generation, Engineering 3 (2017) 365–378.
[5] Y. Wang, J. Zhang, Structural engineering of transition metal-based nanostructured electrocatalysts for efficient water splitting, Front. Chem. Sci. Eng. 12 (2018) 838–854.
[6] D. Wang, Z. Wang, Q. Zhan, Y. Pu, J.-X. Wang, N.R. Foster, L. Dai, Facile and scalable preparation of fluorescent carbon dots for multifunctional applications, Engineering 3 (2017) 402–408.
[7] R. Su, D. Wang, M. Liu, J. Yan, J.-X. Wang, Q. Zhan, Y. Pu, N.R. Foster, J.-F. Chen, Subgram-scale synthesis of biomass waste-derived fluorescent carbon dots in subcritical water for bioimaging, sensing, and solid state patterning, ACS Omega 3 (2018) 13211–13218.
[8] Z. Wang, Y. Pu, D. Wang, J.-X. Wang, J.-F. Chen, Recent advances on metal-free graphene-based catalysts for the production of industrial chemicals, Front. Chem. Sci. Eng. 12 (2018) 855–866.
[9] H.Y. Kim, D.E. Yoon, J. Jang, D. Lee, G.M. Choi, J.H. Chang, J.Y. Lee, D.C. Lee, B.S. Bae, Quantum dot/siloxane composite film exceptionally stable against oxidation under heat and moisture, J. Am. Chem. Soc. 138 (2016) 16478–16485.
[10] Y. Pu, F.H. Cai, D. Wang, J.-X. Wang, J.-F. Chen, Colloidal synthesis of semiconductor quantum dots toward large scale production: a review, Ind. Eng. Chem. Res. 57 (2018) 1790–1802.
[11] J. Leng, J. Chen, D. Wang, J.-X. Wang, Y. Pu, J.-F. Chen, Scalable preparation of Gd_2O_3:Yb^{3+}/Er^{3+} upconversion nanophosphors in a high-gravity rotating packed bed reactor for transparent upconversion luminescent films, Ind. Eng. Chem. Res. 56 (2017) 7977–7983.
[12] Y. Pu, J. Leng, D. Wang, J.-X. Wang, N.R. Foster, J.-F. Chen, Process intensification for scalable synthesis of ytterbium and erbium co-doped sodium yttrium fluoride upconversion nanodispersions, Powder Technol. 340 (2018) 208–216.
[13] Y. Pu, J. Leng, D. Wang, J.-X. Wang, N.R. Foster, J.-F. Chen, Recent progress in the green synthesis of rare-earth doped upconversion nanophosphors for optical bioimaging from cells to animals, Chinese J. Chem. Eng. 26 (2018) 2206–2218.
[14] G.H. Sheetah, Q.K. Liu, B. Senyuk, B. Fleury, I.I. Smalyukh, Electric switching of visible and infrared transmission using liquid crystals co-doped with plasmonic gold nanorods and dichroic dyes, Opt. Express 26 (2018) 22264–22272.
[15] X. He, Z. Wang, Y. Pu, D. Wan, R. Tang, S. Cui, J.-X. Wang, J.-F. Chen, High-gravity-assisted scalable synthesis of zirconia nanodispersion for light emitting diodes encapsulation with enhanced light extraction efficiency, Chem. Eng. Sci. 195 (2019) 1–10.
[16] X. He, R. Tang, Y. Pu, J.-X. Wang, Z. Wang, D. Wang, J.-F. Chen, High-gravity-hydrolysis approach to transparent nanozirconia/silicone encapsulation materials of light emitting diodes devices for healthy lighting, Nano Energy 62 (2019) 1–10.
[17] J.-F. Chen, Green chemical engineering for a better life, Engineering 3 (2017) 279.
[18] H. Liu, T. Hu, D. Wang, J. Shi, J. Zhang, J.-X. Wang, Y. Pu, J.-F. Chen, Preparation of fluorescent waterborne polyurethane nanodispersion by high-gravity miniemulsion polymerization for multifunctional applications, Chem. Eng. Process. 136 (2019) 36–43.
[19] A.S.T. Chiang, The production of dispersible zirconia nanocrystals: a recent patent review, Recent Innovations in Chemical Engineering (Formerly Recent Patents on Chemical Engineering) 7 (2015) 76–95.
[20] J.B. Liu, V. Birss, J. Hill, Electrochemical performance and microstructure characterization of nickel yttrium-stabilized zirconia anode, AICHE J. 56 (2010) 1651–1658.
[21] N. Mahato, A. Banerjee, A. Gupta, S. Omar, K. Balani, Progress in material selection for solid oxide fuel cell technology: a review, Prog. Mater. Sci. 72 (2015) 141–337.
[22] J.R. Kelly, I. Denry, Stabilized zirconia as a structural ceramic: an overview, Dent. Mater. 24 (2008) 289–298.
[23] Y. Xia, C. Zhang, J.-X. Wang, D. Wang, X.F. Zeng, J.-F. Chen, Synthesis of transparent aqueous ZrO_2 nanodispersion with a controllable crystalline phase without modification for a high-refractive-index nanocomposite film, Langmuir 34 (2018) 6806–6813.
[24] K. Enomoto, M. Kikuchi, A. Narumi, S. Kawaguchi, Surface modifier-free organic-inorganic hybridization to produce optically transparent and highly refractive bulk materials composed of epoxy resins and ZrO_2 nanoparticles, ACS Appl.Mater. Inter. 10 (2018) 13985–13998.
[25] C.Y. Wu, K.J. Tu, J.P. Deng, Y.S. Lo, C.H. Wu, Markedly enhanced surface hydroxyl groups of TiO_2 nanoparticles with superior water-dispersibility for photocatalysis, Materials 10 (2017).
[26] C.Y. Wu, K.J. Tu, Y.S. Lo, Y.L. Pang, C.H. Wu, Alkaline hydrogen peroxide treatment for TiO_2 nanoparticles with superior water-dispersibility and visible-light photocatalytic activity, Mater. Chem. Phys. 181 (2016) 82–89.
[27] S.J. Liu, Chemical kinetics of alkaline peroxide brightening of mechanical pulps, Chem. Eng. Sci. 58 (2003) 2229–2244.
[28] C. Alvarez-Vasco, X. Zhang, Alkaline hydrogen peroxide (AHP) pretreatment of softwood: enhanced enzymatic hydrolysability at low peroxide loadings, Biomass Bioenergy 96 (2017) 96–102.
[29] C. Alvarez-Vasco, X. Zhang, Alkaline hydrogen peroxide pretreatment of softwood: hemicellulose degradation pathways, Bioresour. Technol. 150 (2013) 321–327.
[30] Y.P. Su, R.Y. Du, H. Guo, M. Cao, Q.F. Wu, R.X. Su, W. Qi, Z.M. He, Fractional pretreatment of lignocellulose by alkaline hydrogen peroxide: characterization of its major components, Food Bioprod. Process. 94 (2015) 322–330.
[31] Z.H. Ai, N. Wu, L.Z. Zhang, A nonaqueous sol-gel route to highly water dispersible TiO_2 nanocrystals with superior photocatalytic performance, Catal. Today 224 (2014) 180–187.
[32] P.T. Chung, S.H. Chiou, C.Y. Tseng, A.S.T. Chiang, Preparation and evaluation of a zirconia/oligosiloxane nanocomposite for LED encapsulation, ACS Appl. Mater. Inter. 8 (2016) 9986–9993.
[33] G.Y. Guo, Y.L. Chen, New zirconium hydroxide, J. Mater. Sci. 39 (2004) 4039–4043.
[34] M. Allahkarami, J.C. Hanan, Mapping the tetragonal to monoclinic phase transformation in zirconia core dental crowns, Dent. Mater. 27 (2011) 1279–1284.
[35] Y. Kawai, M. Uo, Y.M. Wang, S. Kono, S. Ohnuki, F. Watari, Phase transformation of zirconia ceramics by hydrothermal degradation, Dent. Mater. J. 30 (2011) 286–292.
[36] M.J. Li, Z.C. Feng, P.L. Ying, Q. Xin, C. Li, Phase transformation in the surface region of zirconia and doped zirconia detected by UV Raman spectroscopy, Phys. Chem. Chem. Phys. 5 (2003) 5326–5332.
[37] M.J. Li, Z.H. Feng, G. Xiong, P.L. Ying, Q. Xin, C. Li, Phase transformation in the surface region of zirconia detected by UV Raman spectroscopy, J. Phys. Chem. B 105 (2001) 8107–8111.
[38] V.C. Bachhav, M.A. Aras, Zirconia-based fixed partial dentures: a clinical review, Quintessence Int. 42 (2011) 173–182.
[39] T. Sriamporn, N. Thamrongananskul, C. Busabok, S. Poolthong, M. Uo, J. Tagami, Dental zirconia can be etched by hydrofluoric acid, Dent. Mater. J. 33 (2014) 79–85.
[40] C. Xu, X.G. Qu, Cerium oxide nanoparticle: a remarkably versatile rare earth nanomaterial for biological applications, NPG Asia Mater 6 (2014).
[41] C. Bueno-Ferrer, S. Parres-Esclapez, D. Lozano-Castello, A. Bueno-Lopez, Relationship between surface area and crystal size of pure and doped cerium oxides, J. Rare Earth. 28 (2010) 647–653.
[42] K. Sato, H. Abe, S. Ohara, Selective growth of monoclinic and tetragonal zirconia nanocrystals, J. Am. Chem. Soc. 132 (2010) 2538–2539.
[43] Y.X. Zhang, Z.X. Yang, The mechanism of the high resistance to sulfur poisoning of the rhenium doped nickel/yttria-stabilized zirconia, Appl. Surf. Sci. 447 (2018) 561–568.
[44] T. Gotsch, L. Mayr, M. Stoger-Pollach, B. Klotzer, S. Penner, Preparation and characterization of epitaxially grown unsupported yttria-stabilized zirconia (YSZ) thin films, Appl. Surf. Sci. 331 (2015) 427–436.
[45] R. Sato, S. Ohkuma, Y. Shibuta, F. Shimojo, S. Yamaguchi, Proton migration on hydrated surface of cubic ZrO_2: *ab initio* molecular dynamics simulation, J. Phys. Chem. C 119 (2015) 28925–28933.
[46] S.H. Tang, X.Q. Huang, X.L. Chen, N.F. Zheng, Hollow mesoporous zirconia nanocapsules for drug delivery, Adv. Funct. Mater. 20 (2010) 2442–2447.
[47] E.K. Goharshadi, M. Hadadian, Effect of calcination temperature on structural, vibrational, optical, and rheological properties of zirconia nanoparticles, Ceram. Int. 38 (2012) 1771–1777.
[48] M. Kosmulski, The pH dependent surface charging and points of zero charge. VI. Update, J. Colloid Interf. Sci. 426 (2014) 209–212.
[49] D.H. Shen, N. Horiuchi, S. Nozaki, M. Miyashin, K. Yamashita, A. Nagai, Synthesis and enhanced bone regeneration of carbonate substituted octacalcium phosphate, Bio-Med. Mater. Eng. 28 (2017) 9–21.
[50] D. Yang, Y.B. Li, Y.G. Wang, Z.Y. Jiang, Bioinspired synthesis of mesoporous ZrO_2 nanomaterials with elevated defluoridation performance in agarose gels, RSC Adv. 4 (2014) 49811–49818.
[51] S. Mallakpour, A.N. Ezhieh, Polymer nanocomposites based on modified ZrO_2 NPs and poly(vinyl alcohol)/poly(vinyl pyrrolidone) blend: optical, morphological, and thermal properties, Polym-Plast. Technol. 56 (2017) 1136–1145.

[52] X.H. Hou, K.L. Choy, N. Brun, V. Serin, Nanocomposite coatings codeposited with nanoparticles using aerosol-assisted chemical vapour deposition, J. Nanomater. 2013 (2013) 219039.
[53] M. Banik, T. Basu, Calcium phosphate nanoparticles: a study of their synthesis, characterization and mode of interaction with salmon testis DNA, Dalton T 43 (2014) 3244–3259.
[54] I. Arrizabalaga, O. Gomez-Laserna, J.A. Carrero, J. Bustamante, A. Rodriguez, G. Arana, J.M. Madariaga, Diffuse reflectance FTIR database for the interpretation of the spectra obtained with a handheld device on built heritage materials, Anal. Methods-UK 7 (2015) 1061–1070.
[55] J.D. Pasteris, C.H. Yoder, M.P. Sternlieb, S. Liu, Effect of carbonate incorporation on the hydroxyl content of hydroxylapatite, Mineral. Mag. 76 (2012) 2741–2759.
[56] S.N. Basahel, T.T. Ali, M. Mokhtar, K. Narasimharao, Influence of crystal structure of nanosized ZrO_2 on photocatalytic degradation of methyl orange, Nanoscale Res. Lett. 10 (2015).
[57] S. Gredelj, A.R. Gerson, S. Kumar, G.P. Cavallaro, Characterization of aluminium surfaces with and without plasma nitriding by X-ray photoelectron spectroscopy, Appl. Surf. Sci. 174 (2001) 240–250.
[58] J.A. Navio, M.C. Hidalgo, G. Colon, S.G. Botta, M.I. Litter, Preparation and physicochemical properties of ZrO_2 and Fe/ZrO_2 prepared by a sol-gel technique, Langmuir 17 (2001) 202–210.
[59] S. Sugumaran, C.S. Bellan, Transparent nano composite PVA-TiO_2 and PMMA-TiO_2 thin films: optical and dielectric properties, Optik 125 (2014) 5128–5133.
[60] A. Maurya, P. Chauhan, Synthesis and characterization of sol-gel derived PVA-titanium dioxide (TiO_2) nanocomposite, Polym. Bull. 68 (2012) 961–972.
[61] C.L. Lu, B. Yang, High refractive index organic-inorganic nanocomposites: design, synthesis and application, J. Mater. Chem. 19 (2009) 2884–2901.
[62] K. Krishnamoorthy, S. Natarajan, S.J. Kim, J. Kadarkaraithangam, Enhancement in thermal and tensile properties of ZrO_2/poly(vinyl alcohol) nanocomposite film, Mater. Express 1 (2011) 329–335.